

# Almost strong $0, \pi$ edge modes in clean, interacting 1D Floquet systems

Daniel J. Yates<sup>1</sup>, Fabian H.L. Essler<sup>2</sup>, and Aditi Mitra<sup>1</sup>

<sup>1</sup>*Center for Quantum Phenomena, Department of Physics,  
New York University, 726 Broadway, New York, NY, 10003, USA*

<sup>2</sup>*Rudolf Peierls Centre for Theoretical Physics, University of Oxford, Oxford OX1 3PU, UK*

(Dated: January 28, 2020)

Certain periodically driven quantum many-particle systems in one dimension are known to exhibit edge modes that are related to topological properties and lead to approximate degeneracies of the Floquet spectrum. A similar situation occurs in spin chains, where stable edge modes were shown to exist at all energies in certain integrable spin chains. Moreover, these edge modes were found to be remarkably stable to perturbations. Here we investigate the stability of edge modes in interacting, periodically driven, clean systems. We introduce a model that features edge modes that persist over times scales well in excess of the time needed for the bulk of the system to heat to infinite temperatures.

## I. INTRODUCTION

Non-abelian edge modes have attracted considerable attention as a possible route to quantum information processing<sup>1–5</sup>. Such edge modes occur in the ground state sector of various models, and information encoded in them is protected by a finite gap to excitations. In a series of recent works<sup>6–10</sup> it was established that, remarkably, certain spin models support topological edge modes at all energy densities that are either stable or very long-lived. Stable edge modes were termed *strong zero modes* in Ref. 6 and are a reflection of the existence of an operator  $\Psi_0$  that commutes with the Hamiltonian  $H$  in the thermodynamic limit, anti-commutes with a discrete (say  $\mathbb{Z}_2$ ) symmetry of the Hamiltonian  $\mathcal{D}$ ,  $\{\Psi_0, \mathcal{D}\} = 0$ , and is normalizable  $\Psi_0^2 = O(1)$ . The presence of a strong zero mode implies a parameter regime where the entire spectrum of the Hamiltonian is approximately doubly degenerate, with the almost degenerate eigenstates being  $\{|n\rangle, \Psi_0|n\rangle\}$ , and correspond to two different discrete symmetry sectors.

Strong zero modes were shown to exist in the transverse field Ising model, which has a free fermionic spectrum, and in the XYZ spin chain<sup>6</sup>, which is an interacting integrable theory. Importantly, these edge features were shown to be extremely robust to perturbations about these limits in the sense that *almost strong zero modes* with long but finite life times persist<sup>7</sup>. Edge modes that lead to approximate degeneracies at all energies are also known to occur in periodically driven systems<sup>11–16</sup> and are closely related to symmetry-protected topological (SPT) phases<sup>17–23</sup>.

By virtue of the periodicity of the spectrum of the (stroboscopic) time evolution operator  $U(T)$  the resulting structure of edge modes is richer than in the equilibrium case: in addition to (almost) zero energy modes there are so-called  $\pi$ -modes, which correspond to a quasi-energy  $\epsilon \approx \pm\pi/T$ , where  $T$  is the period of the drive. In the terminology introduced above this corresponds to the existence of two operators  $\Psi_0$  and  $\Psi_\pi$  that are normalizable,  $\Psi_{0,\pi}^2 = O(1)$ , anti-commute with a discrete symmetry of the system  $\{\Psi_{0,\pi}, \mathcal{D}\} = 0$  and respec-

tively approximately commute  $[\Psi_0, U(T)] \approx 0$  or anti-commute  $\{\Psi_\pi, U(T)\} \approx 0$  with the time evolution operator  $U(T)$ . In terms of the spectrum of the Floquet Hamiltonian the existence of  $\Psi_0$  implies the presence of pairs of almost degenerate eigenstates  $\{|n\rangle, \Psi_0|n\rangle\}$ , while the existence of  $\Psi_\pi$  implies the existence of pairs of eigenstates  $\{|n\rangle, \Psi_\pi|n\rangle\}$  whose energies (approximately) differ by  $\pi/T$ .

The existence of strong zero and  $\pi$  mode operators in non-interacting periodically driven models<sup>11</sup>, in the high-frequency limit<sup>18</sup>, and in the Floquet-many body localization context<sup>12,13,15,16,24</sup>, has been studied. In the high-frequency regime the Floquet Hamiltonians typically studied in the literature become short-ranged and the situation becomes very similar to the equilibrium case<sup>7</sup>. The question of what happens in interacting, clean Floquet systems away from the high-frequency regime has not yet been explored in any detail. In Ref. 14 it was shown that edge modes lead to approximate degeneracies in the Floquet spectrum of a particular clean, interacting system. However the implications of this for the dynamics of the modes and their robustness to heating was not investigated.

Periodically driven clean systems are known to heat up<sup>25–29</sup> and are generically characterized by Floquet Hamiltonians with long-ranged interactions, so that one would not expect long-lived edge modes to exist at all energy densities. We show that in contrast to this expectation there exist periodically driven interacting systems that feature almost strong zero and  $\pi$  modes at all energy densities, even though the system heats on much shorter time scales.

The paper is organized as follows. Section II presents results for the strong modes for a free Floquet system. Section III presents results for the almost strong modes of the interacting Floquet system. Section IV derives effective interacting Floquet Hamiltonians around some exactly solvable limits, and compares almost strong modes obtained from them to that obtained from the full time-evolution. Section V presents the conclusions. The details of the analytic calculations and additional discussions are relegated to the Appendices.

## II. STRONG ZERO AND $\pi$ MODES FOR THE FREE BINARY DRIVE

It is instructive to explicitly construct the strong zero and  $\pi$  mode operators for periodically driven systems with Floquet Hamiltonians that can be expressed as fermion bilinears. As an example we consider an Ising binary drive which switches between two Hamiltonians for equal durations  $T/2$ <sup>11,13,23,30</sup>,

$$U(T) = e^{-\frac{iTJ_x}{2}H_{xx}}e^{-\frac{iT\mu}{2}H_z},$$

$$H_{xx} = \sum_{i=1}^L \sigma_i^x \sigma_{i+1}^x, \quad H_z = \sum_{i=1}^L \sigma_i^z. \quad (1)$$

In the following we set  $J_x = 1$ . The model (1) has a  $\mathbb{Z}_2$  symmetry of rotations around the  $z$ -axis by 180 degrees, generated by  $\mathcal{D} = \sigma_1^z \sigma_2^z \dots \sigma_L^z$ . We now construct operators  $\Psi_{0,\pi}$  that are localized at the boundaries such that  $U^\dagger(T)\Psi_{0,\pi}U(T) = \pm\Psi_{0,\pi}$ , with an error that is exponentially suppressed in the system size  $L$ . It is convenient to introduce Majorana fermions  $a_{2\ell-1} = \prod_{j=1}^{\ell-1} \sigma_j^z \sigma_\ell^x$  and  $a_{2\ell} = \prod_{j=1}^{\ell-1} \sigma_j^z \sigma_\ell^y$ , and collect the even and odd labeled Majoranas into two vectors  $\vec{a}_{\text{odd}} = (a_1, a_3, \dots, a_{2L-1})$ ,  $\vec{a}_{\text{even}} = (a_2, a_4, \dots, a_{2L})$ . Both  $H_{xx}$  and  $H_z$  are quadratic in the Majorana operators, and concomitantly their stroboscopic time evolution can be cast in the form

$$\begin{pmatrix} \vec{a}_{\text{odd}}((n+1)T) \\ \vec{a}_{\text{even}}((n+1)T) \end{pmatrix} = M \begin{pmatrix} \vec{a}_{\text{odd}}(nT) \\ \vec{a}_{\text{even}}(nT) \end{pmatrix}, \quad (2)$$

where  $M$  is an orthogonal matrix, and is given in Appendix A. We then make the Ansatz  $\Psi_{0,\pi} = \sum_j \varphi_j^{(0,\pi)} a_j$  for the zero/ $\pi$ -mode operators and require them to be invariant (up to a sign in case of the  $\pi$ -mode) under stroboscopic time evolution. This leads to an eigenvalue equation of the form  $\varphi_j^{(\sigma)} = \cos(\sigma) \sum_\ell M_{j\ell} \varphi_\ell^{(\sigma)}$ . Interestingly, these equations can essentially be solved in closed form (Appendix A) in the limit of large system size  $L$ .

Dropping contributions that are exponentially small in system size, the operators can be written in the form  $\Psi_\sigma \approx \Psi_\sigma^L + \Psi_\sigma^R$ , where  $\Psi_\sigma^L$  ( $\Psi_\sigma^R$ ) has support mainly near the left (right) boundary, where

$$\Psi_0^L = \sum_{j \geq 1} \epsilon_-^{j-1} \left[ \cos\left(\frac{T\mu}{2}\right) a_{2j-1} - \sin\left(\frac{T\mu}{2}\right) a_{2j} \right],$$

$$\Psi_\pi^L = \sum_{j \geq 1} \epsilon_+^{j-1} \left[ \sin\left(\frac{T\mu}{2}\right) a_{2j-1} + \cos\left(\frac{T\mu}{2}\right) a_{2j} \right]. \quad (3)$$

Here we have defined  $\epsilon_- = \tan(\frac{T\mu}{2}) \cot(\frac{TJ_x}{2})$  and  $\epsilon_+ = -\cot(\frac{T\mu}{2}) \cot(\frac{TJ_x}{2})$ . Similar  $0, \pi$  mode operators appear in Ref. 11 for a time-symmetrized version of  $U(T)$ . Both modes can be readily seen to anticommute with the generator of the  $\mathbb{Z}_2$  symmetry  $\{\mathcal{D}, \Psi_{0,\pi}\} = 0$ , which establishes that acting with  $\Psi_{0,\pi}$  on an eigenstate of  $U(T)$  that is even (odd) under the  $\mathbb{Z}_2$  symmetry gives an eigenstate  $U(T)$  that is odd (even). The condition for  $\Psi_\sigma$  to be

normalizable in the thermodynamic limit is  $|\epsilon_\sigma| < 1$  and  $|\epsilon_\sigma| = 1$  fixes the location of the topological phase transitions of the model *cf.* Fig. 1. Here the topological phases are that of a free BDI Floquet SPT<sup>19–23</sup> with an invariant in  $\mathbb{Z} \times \mathbb{Z}$ , the two integers being the numbers of  $0, \pi$  edge modes. The drive used in this paper only generates indices of 0 or 1 for each edge mode species so that the difference between  $(\mathbb{Z}_2 \times \mathbb{Z}_2)$  and  $(\mathbb{Z} \times \mathbb{Z})$  is not apparent. More general drives that preserve the BDI symmetries can realize a larger numbers of edge modes in both species<sup>11,31–33</sup>. Whether these additional edge modes are associated with additional strong mode operators is left for future study.

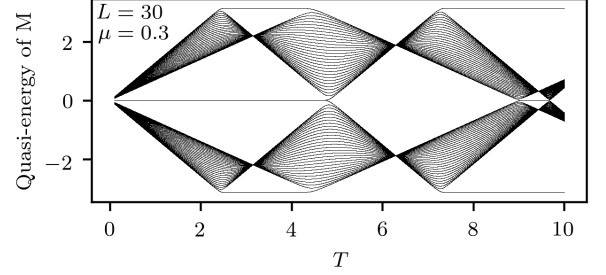


FIG. 1. Quasi-energies obtained from the eigenvalues of  $M$  for the free binary drive. Different topological phases are visible as the drive period  $T$  is varied. From left to right, the phases are  $M_0$ ,  $M_0 + M_\pi$ , trivial, and  $M_\pi$ , where  $M_\sigma$  indicates the existence of a strong Majorana edge mode, *cf.* Eqn. (3).

In the  $T \rightarrow 0$  limit, we can perform a high-frequency expansion<sup>34,35</sup> to leading order and obtain the Floquet Hamiltonian  $H_F = \frac{1}{2}(J_x H_{xx} + \mu H_z)$ , which is a transverse field Ising model. In this limit our expression (3) for the zero mode  $\Psi_0$  reduces to that previously obtained in equilibrium<sup>1,6,8</sup>. It is instructive to consider the strong edge modes in some simple limiting cases<sup>23</sup>.

### 1. $T\mu = (2n+1)\pi$ and $TJ_x$ arbitrary

Here  $\exp(-iT\mu H_z/2) = (-i(-1)^n)^L \mathcal{D}$  and  $\sigma_1^x$  becomes a strong  $\pi$  mode, while there is no strong zero mode. This is consistent with  $\epsilon_- \rightarrow \infty$ , which signals to non-normalizability of our zero mode solution. Only the first term in the expansion of  $\Psi_\pi^L$  in Eq. (3) is non-zero and gives  $\psi_\pi^L = \sigma_1^x$ .

### 2. $T\mu = 2n\pi$ and $TJ_x$ arbitrary

In this case we have  $\exp(-iT\mu H_z/2) = 1$  and  $\sigma_1^x$  becomes a strong zero mode, whereas there is no strong  $\pi$  mode. This corresponds to the limit  $\epsilon_+ \rightarrow \infty, \epsilon_- \rightarrow 0$  in (3).

### 3. $TJ_x = (2n+1)\pi$ and $T\mu$ arbitrary

Then  $\exp(-iTJ_x H_{xx}/2) = (-i(-1)^n)^{L-1} \sigma_1^x \sigma_L^x$  and it is straightforward to check that both a strong 0 and  $\pi$  mode exist. Their explicit expressions are given by the  $j = 1$  terms in (3).

#### 4. $TJ_x = 2n\pi$ and $T\mu$ arbitrary

Here we have  $\exp(-iTJ_x H_{xx}/2) = 1$  and no strong edge modes exist unless  $T\mu/\pi$  is an integer. If this integer is odd (even) then  $\sigma_1^x$  is a strong  $\pi$  (zero) mode.

### III. INTERACTING TERNARY DRIVE

We now add interactions to the Floquet driving by dividing the period into 3 equal parts

$$U(T) = e^{-i\frac{TJ_z}{3}H_{zz}} e^{-i\frac{TJ_x}{3}H_{xx}} e^{-i\frac{T\mu}{3}H_z}, \quad (4)$$

where  $H_{zz} = \sum_{i=1}^{L-1} \sigma_i^z \sigma_{i+1}^z$ . We note that  $\mathcal{D}$  remains a symmetry of this drive. We have studied this model by means of exact diagonalization on system sizes up to  $L = 14$ . In the following we set  $J_x = 1$ . It is useful to define  $T'$  as  $T'/2 = T/3$  so that when  $J_z \rightarrow 0$  the ternary drive reduces to the solvable binary drive. This facilitates comparisons between results for free (Figs. 1 and 3) and interacting drives (Figs. 2 and 4). Guided by the findings of Ref. 7 in equilibrium we wish to investigate the possible existence of almost strong zero and  $\pi$  modes, i.e. long-lived edge modes. In order to search for these modes we consider the overlap of the boundary spin  $\sigma_1^x = a_1$  at time  $nT$  with the boundary spin at time zero

$$A(nT) = \frac{1}{2L} \text{Tr}[\sigma_1^x(nT)\sigma_1^x] = \frac{1}{2L} \text{Tr}[a_1(nT)a_1]. \quad (5)$$

In the absence of any edge modes  $A(nT)$  is expected to rapidly decay to zero. On the other hand, almost strong zero or  $\pi$  modes will have a non-zero overlap with the edge spin  $\text{Tr}[\sigma_1^x \Psi_{0,\pi}] \neq 0$  and this prevents  $A(nT)$  from decaying to zero rapidly with time. The rationale behind these expectations is discussed in Appendix B.

An alternative diagnostic of edge modes is the auto-correlation function measured with respect to a certain initial state  $|\psi\rangle$ , defined as  $A_\psi(nT) = \langle\psi|\sigma_1^x(nT)\sigma_1^x|\psi\rangle$ . The physical meaning of this quantity is that we start from an initial state  $|\psi\rangle$ , flip a spin at site 1, then time-evolve until time  $nT$ , and flip the spin back again obtaining a state  $\sigma_1^x U(nT) \sigma_1^x |\psi\rangle$ .  $A_\psi(nT)$  then measures the overlap of this state with one where the initial state was evolved up to time  $nT$  without any spin-flips  $U(nT)|\psi\rangle$ . Thus this quantity measures the decoherence of any edge mode. If almost strong modes exist, then after an initial transient the two quantities  $A(nT), A_\psi(nT)$  behave similarly (Appendix B).

In Fig. 2 we show results for  $A(nT)$  as a function of stroboscopic time  $nT$  and drive period  $T$  for parameters  $\mu = 0.3$  and  $J_z = 0.1$ . We see that edge modes persist for considerable time even in the presence of interactions. For the parameters shown, these modes are adiabatically connected to the free case. In the remainder of the paper we analyze this behavior as a function of system size  $L$ , drive frequency  $T^{-1}$ , and strength of interactions  $J_z$ .

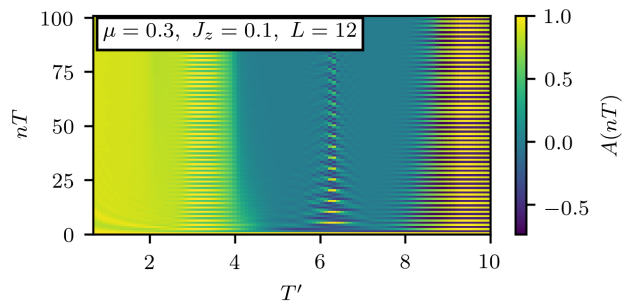


FIG. 2. Edge mode diagnostic  $A(nT)$  for the interacting ternary drive with period  $T$  where  $T' = 2T/3$ . There are three parameter regimes in which almost strong edge modes occur:  $M_0$  ( $T'J_x < 2$ ),  $M_0 + M_\pi$  ( $2 < T'J_x < 4$ ) and  $M_\pi$  ( $8 < T'J_x$ ). Here  $M_{0,\pi}$  indicates the presence of a edge zero/ $\pi$  mode. The structure seen at  $T' \approx 2\pi$  arises due to the flat band section visible in Fig. 1 and the small value of  $J_z = 0.1$ . A larger  $J_z$  would quickly dampen these oscillations. The oscillatory behavior in the regime  $n \lesssim 10$  and  $T' \lesssim 2$  is a finite-size effect: the system size,  $L = 12$ , is too small for the spectrum to “wrap around” the unit circle for these high frequencies, cf. Fig. 15.

Since the  $\pi$ -modes alternate sign every period, their persistence with time and system size is most apparent in a staggered average over adjacent stroboscopic times,  $A^-(nT) = [A(nT) - A((n+1)T)]/2$ . It is similarly convenient to extract the effects of zero modes by considering the flat average  $A^+(nT) = [A(nT) + A((n+1)T)]/2$ . To set the stage we first investigate the behavior of  $A^\pm$  for the free binary drive, where we know when strong edge modes exist. In Fig. 3 we show results for  $|A^\pm(nT)|$  for parameters where (i) a strong zero mode exists (top panel); (ii) strong zero and  $\pi$  modes coexist (middle panel); and (iii) only a strong  $\pi$  mode exists. It is apparent from the top and bottom panels that in the absence of the respective strong edge mode, the corresponding diagnostic rapidly decays to zero, and this behavior is system size independent. In contrast, when a strong edge mode exists, the diagnostic stays constant on a time scale that grows with system size. Fig. 3 also reveals how the system rebounds after the “decay”, revealing recurrences characteristic of a free system. The log scale of the  $x$ -axis masks the fact that the decays in the free system are simple cosine oscillations that are exponentially slow in system size.

We now turn to the ternary drive. Results for the edge mode diagnostics for  $J_z/J_x = 0.05$  are shown in Fig. 4. We observe almost strong edge modes with life times that initially grow with system size and eventually saturate. We note that going from the top to the bottom panels the drive frequency is being lowered, and this changes the life times of the almost strong edge modes. In particular we see that for sufficiently low frequency driving (middle and lower panels) the life times of the almost strong modes saturate at increasingly lower system sizes.

An immediate question raised by the existence of long-

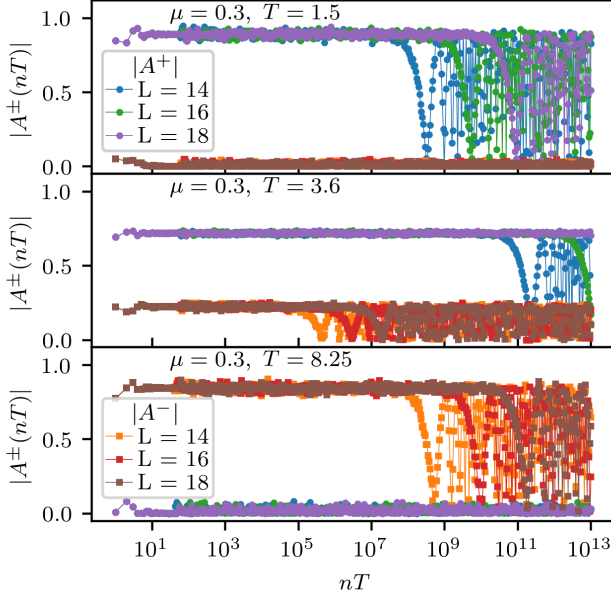


FIG. 3. Suitably symmetrized/anti-symmetrized overlaps  $A^\pm$  as a function of stroboscopic time  $nT$ , for the binary drive. Top panel: a strong zero mode exists. Middle panel: a strong zero mode coexists with a strong  $\pi$  mode. Lower panel: Only a strong  $\pi$  mode exists. The lifetimes of the modes grow exponentially with system size. From top to bottom panels, all parameters are fixed, and only the drive frequency  $T^{-1}$  is decreased.

lived edge modes is whether they are related to some kind of prethermal behavior<sup>36–44</sup>. To answer this question we have investigated on what time scales heating occurs in our system. We now show that the lifetime of the modes far exceeds thermalization times by several orders of magnitude.

The comparison between the lifetime of almost strong modes, and thermalization times are presented in Figs. 5 and 6. Fig. 5 presents results for two different parameter points coinciding with the existence of almost strong zero modes,  $T = 1.5$  on the left panels,  $T = 2.0$  on the right panels, and  $\mu = 0.2, J_z = 0.3$  for both. In the top panels of Fig. 5 we show the behavior of  $|A^+(nT)|$  as a function of stroboscopic time for several system sizes and parameters that correspond to two different periods. For these parameters  $A^- \approx 0$  within a cycle. We observe that  $|A^+(nT)|$  remains large for a substantial but finite time, indicating the existence of an almost strong zero mode. For the parameters chosen in Fig. 5, system size of  $L = 14$  is sufficient to show the saturation of the lifetime with system size.

The lower two panels in Fig. 5 show the time-evolution of two measures of thermalization, namely the entanglement entropy density for a subsystem of size three and the expectation value of  $\sigma_{j=L/2}^z$  at the center of the chain, both following a quantum quench from a Néel initial state. These results show that the system heats to

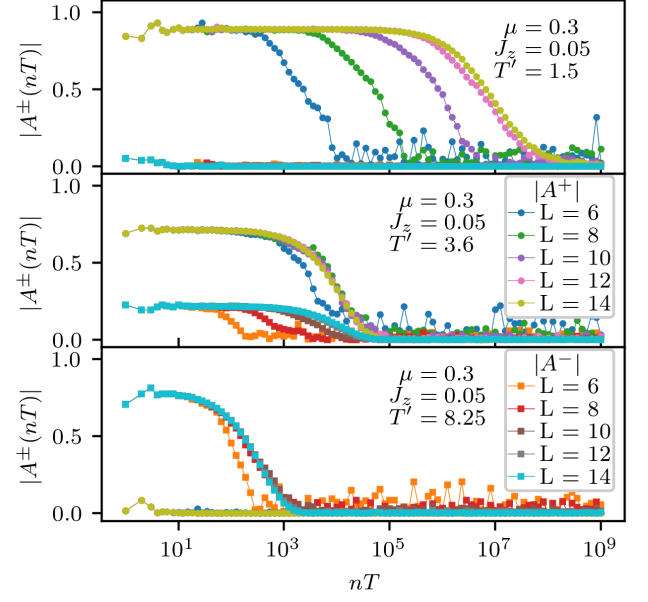


FIG. 4. Suitably symmetrized/anti-symmetrized overlaps  $A^\pm$  as a function of stroboscopic time  $nT$ , for the interacting ternary drive with  $J_z/J_x = 0.05$ , and the same  $T', \mu$  as for the binary drive shown in Fig. 3. Note that the  $T'$  here equals the  $T$  in figure 3. Top panel: an almost strong zero mode exists whose lifetime grows with system size, and does not saturate for the sizes shown. Middle panel: almost strong zero and  $\pi$  modes coexist. The life time of the zero ( $\pi$ ) mode saturates for system  $L = 8$  ( $L = 12$ ). Lower panel: there is an almost strong  $\pi$  mode, whose lifetime saturates for system size  $L = 8$ .

infinite temperature on a much shorter time scale than the lifetimes of the edge modes. Note that at sufficiently late times the entanglement entropy density approaches the infinite temperature limit of  $\ln(2)$  (dashed line) as the system size is increased, *cf.* Fig. 8. We focus on subsystem size three as this is the maximal value for which finite-size effects (due to the limited system size  $L$ ) are sufficiently small. We find that the behavior of the  $\sigma_j^z$  at other positions is qualitatively similar in that it rapidly decays to zero, including at the edge. We have considered several other initial states and observed the same behavior.

In Fig. 6 we present analogous results for a parameter regime in which an almost strong  $\pi$  mode exists (left hand panels) and a case in which there are no long-lived edge modes (right hand panels). The results for the entanglement entropy density and the central spin show that in both cases the system quickly heats to an infinite temperature state. For  $T = 3.1, J_z = 0.3$  and  $\mu = 1.5$  (left hand panel) the results for  $A^-(nT)$  reveal the existence of a  $\pi$  edge mode long after the system has thermalized. On the other hand, for  $T = 1.5, J_z = 0.3$  and  $\mu = 1.5$  (right hand panel) the edge coherence disappears around the same time when the system reaches an infinite temperature state. We observe that upon decreasing  $J_z$  the lifetimes of existing zero or  $\pi$  modes will increase roughly

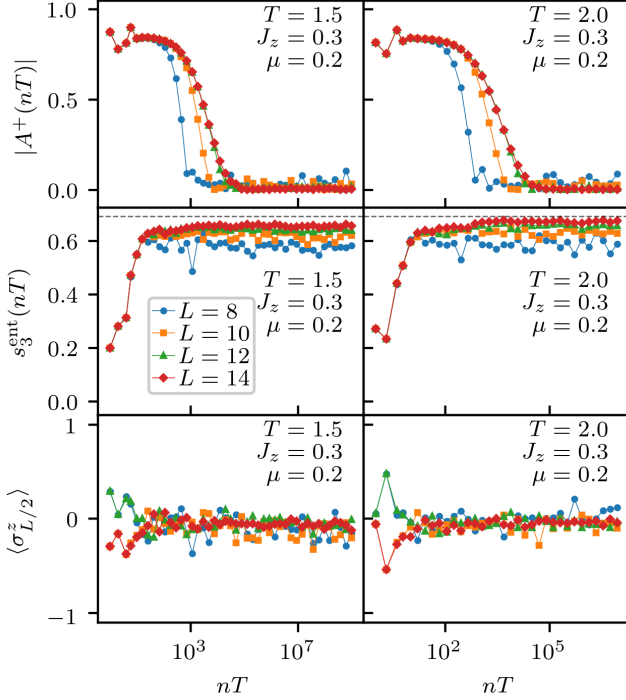


FIG. 5. Top panels: Time-evolution of edge zero mode diagnostic  $A^+(nT)$  ( $A^-(nT) \approx 0$ , not shown). Middle and lower panels: Time-evolution of the three-site entanglement-entropy density and expectation value of the central spin  $\langle \sigma_{j=L/2}^z(nT) \rangle$  for a system initialized in a classical Néel state. Middle and lower panels show thermalization on time-scales that do not depend on system size, and occur on time-scales much shorter than the lifetime of the almost strong mode in the upper panel.

as  $\sim \exp(1/J_z)$ . It is difficult to quantify this behavior more precisely due to the limitations set by the system sizes accessible to us. We typically find only a narrow parameter range in which  $J_z$  can be varied while the lifetimes of zero/ $\pi$  modes still saturate for  $L = 14$ . We find that the lifetimes of both zero and  $\pi$  modes can be extended by moving closer to their respective integrable lines, i.e. the centers of the blue and red regions in Fig. 7.

A second diagnostic for detecting the presence of edge modes is the overlap of  $\sigma_1^x$  between opposite symmetry sectors<sup>7</sup>. This is defined as

$$\Gamma = \frac{1}{2L} \sum_s \max_{s'} |\langle s | \sigma_1^x | s' \rangle|^2, \quad (6)$$

where  $|s\rangle$  and  $|s'\rangle$  denote the exact eigenstates of the Floquet unitary  $U(T)$ . This diagnostic, since it takes a mean of the overlap between opposite symmetry sectors, treats zero and  $\pi$  modes on an equal footing. The reasoning why  $\Gamma$  is a useful edge mode diagnostic goes as follows. Up to corrections that are exponentially small in system size strong edge modes  $\Psi_{0,\pi}$  map each eigenstate  $|s\rangle$  to another eigenstate of opposite fermion parity, i.e.  $|s'\rangle \approx \Psi_{0,\pi}|s\rangle$ . As  $\text{Tr}(\sigma_1^x \Psi_{0,\pi}) = \mathcal{O}(1)$  strong edge modes

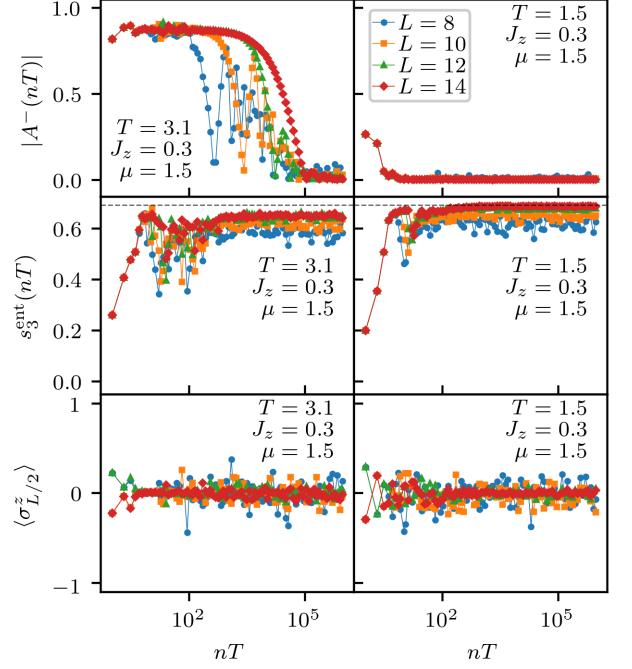


FIG. 6. Top panels: almost strong  $\pi$ -mode diagnostic  $A^-(nT)$  for two low frequency drives as a function of time. For  $T = 3.1$  there is a long-lived  $\pi$ -mode up to times  $nT \sim 10^5$ , while for  $T = 1.5$  there isn't. ( $A^+ \approx 0$ , for both cases, not shown) Middle and bottom panels: time evolution of the three-site entanglement-entropy density  $s_3^{\text{ent}}(nT)$  and average spin  $\langle \sigma_{j=L/2}^z(nT) \rangle$  starting from a Néel state. The system is seen to approach an infinite temperature state for times of the order of  $nT \sim 10$  for both parameter sets.

therefore lead to finite values of  $\Gamma$ . Reversing the argument, the exponentially small factor  $2^{-L}$  in the definition of  $\Gamma$  can be compensated only if most eigenstates  $|s\rangle$  of  $U(T)$  have a partner  $|s'\rangle$  in the opposite symmetry sector such that  $|\langle s | \sigma_1^x | s' \rangle|^2 = \mathcal{O}(1)$ . As almost all eigenstates of  $U(T)$  have finite correlation lengths this implies the existence of fermionic edge modes. We plot  $\Gamma$  as a function of the parameters  $T'$  and  $\mu$  of the ternary drive for fixed substantial interaction strengths  $J_z/J_x = 0.2, 3.0$  in Fig. 7. We observe almost strong edge modes despite the Floquet Hamiltonian having sizeable interactions. For comparison we show the regions in which strong edge modes exist in the binary drive. For the system sizes accessible to us, the size and shape of the black regions that indicate the presence of edge modes are only weakly affected by finite-size effects (Appendix C).

### A. Finite size effects

In a large finite system local thermalization<sup>45</sup> implies that the difference between the time average of the system's reduced density matrix  $\overline{\rho_A}$ , and an appropriate



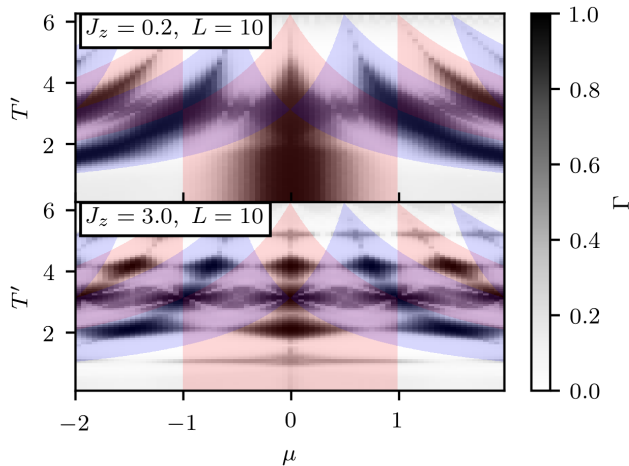


FIG. 7. Edge mode diagnostic  $\Gamma$  for fixed  $J_z/J_x = 0.2, 3.0$ . The black regions indicate the presence of almost strong edge modes. For comparison we also indicate where zero (red) and  $\pi$ -modes (blue) exist in the binary drive model. In the top panel, the strong zero mode for  $|\mu| \leq 1$  and sufficiently small  $T$  is closely connected to the topological phase of the static Kitaev chain. The blue and red wings for  $T > 0$  are introduced by the Floquet driving and do not have a static analog.

thermal reduced density matrix  $\rho_A^{\text{th}}$ , goes to zero as system size is increased for a fixed choice of subsystem  $A$

$$|\overline{\rho_A} - \rho_A^{\text{th}}| < \epsilon_L, \quad \lim_{L \rightarrow \infty} \epsilon_L = 0. \quad (7)$$

This means in particular that the time-averages of expectation values of local observables, sufficiently far away from any boundaries, approach thermal values as the system size is increased. We will now show that our system quickly reaches an infinite temperature steady state in this sense. Our discussion necessarily focusses on small subsystems, and we are in particular unable to address questions such as how the time scale at which the reduced density matrix of a large subsystem (but still small compared to the system size  $L$ ), approaches its infinite temperature value within a given error, depends on the size of the subsystem. However, given that the correlation lengths in our system are very short, all “large” observables are already accessible in short subsystems. Considering how close a two point function at separation 100 is to its infinite temperature value is essentially a purely academic question.

In the following we focus on two representative local quantities, namely the  $z$ -component of the spin in the centre of our chain and the entanglement entropies of small subsystems. Fig. 8 shows the very late time average of the entanglement entropy per site as a function of inverse system size  $1/L$  for several subsystem sizes  $L_A$ . We see that for the system sizes accessible to us  $s_{L_A}^{\text{ent}}(\infty)$  approaches the infinite temperature value  $\log(2)$ . This is of course as expected, but it allows us to quantify the

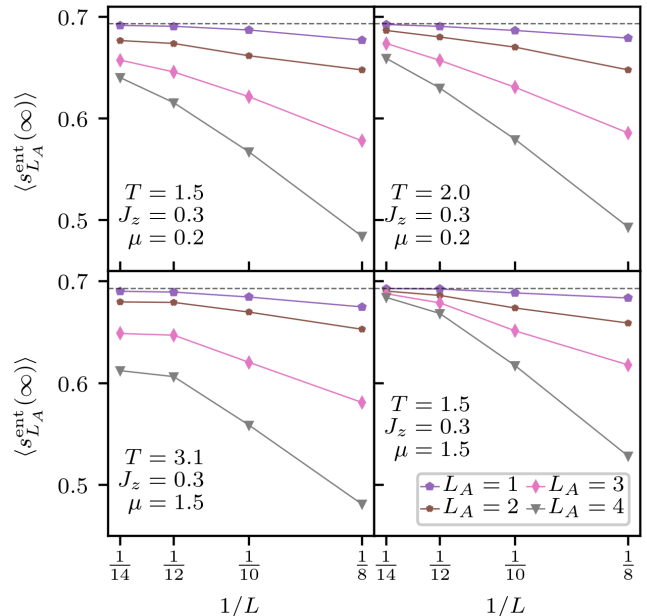


FIG. 8. Entanglement entropy density for different subsystem sizes  $L_A$  starting from the left end, and averaged over 100 time points from  $10^9 - 10^{12}$ , long after the edge modes have melted. There is a clear trend towards the infinite temperature value of  $\log(2)$ , dashed line, as the chain length  $L$  is increased.

role of finite-size effects. In Fig. 9 we show the difference between the entanglement entropy per site at finite times and the late time average  $s_{L_A}^{\text{ent}}(\infty)$ . We see that  $s_{L_A}^{\text{ent}}(t)$  approaches its late time value, which we have just argued to correspond to an infinite temperature state, on time scales that are much shorter than the life times of the edge modes. We note that reducing  $J_z$  will extend the lifetime of the edge modes as discussed above, but not change the time scales shown in Fig. 9. In Fig. 10 we show the fluctuations of  $\langle \sigma_{L/2}^z \rangle$  at late times. We see that as the system size  $L$  is increased, fluctuations around the infinite temperature value of zero are suppressed.

Inspection of Figs. 8, 10, and 9 reveals that for parameters  $T = 3.1$ ,  $J_z = 0.3$ ,  $\mu = 1.5$ , deviations from the infinite temperature values are larger and convergence is slower. This should be seen in the context that the lifetime of the  $\pi$  edge mode in this case has not yet saturated for system size  $L = 14$ , cf. Fig. 6. So while our finite-size analysis is less conclusive in this case, our findings are compatible with the general picture of local thermalization to an infinite temperature state long before the edge modes start to decay.

#### IV. FLOQUET HAMILTONIAN

It is instructive to investigate the existence of edge modes at the level of the stroboscopic Floquet Hamilto-

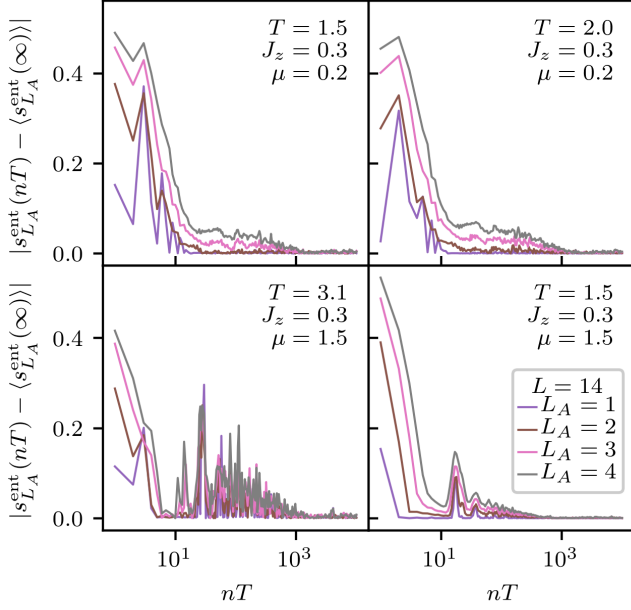


FIG. 9. Short time entanglement entropy density for different subsystem sizes  $L_A$ , starting from the left end, for  $L = 14$ . Plotted is the difference of the entanglement density from the very late entanglement density used in figure 8, where the latter is long after the edge modes have melted.

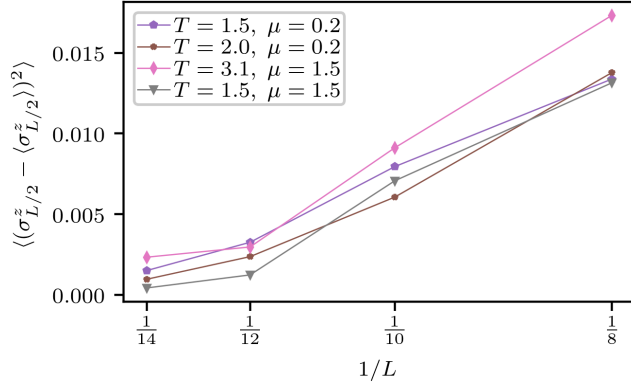


FIG. 10. Fluctuations of  $\langle \sigma_{L/2}^z \rangle$  after the initial decay. The average is taken over the last 40 time points visible in Figs. 5, 6.

nian obtained from  $U(T) = e^{-iTH_F}$ . We extract effective Floquet Hamiltonians around two limits, high and low frequencies. As we are ultimately interested in the behavior of large but finite systems, and short and intermediate times, we set aside the issue of the convergence of such expansions. In the small  $T$  limit of off-resonant driving, our Floquet Hamiltonian is interacting and non-integrable

$$H_F \approx H_F^{(0)} = \frac{1}{3} (J_z H_{zz} + J_x H_{xx} + \mu H_z). \quad (8)$$

A quantitative measure of how well  $H_F^{(0)}$  reproduces the time evolution is provided by the normalized Frobenius norm of the difference of evolution operators  $\Delta(nT) = U(nT) - e^{-inTH_F^{(0)}}$

$$\Delta U(nT) = \frac{1}{2^L} \sqrt{\text{tr} [(\Delta(nT))^\dagger \Delta(nT)]}. \quad (9)$$

Fig. 11 shows that the dynamics induced by  $H_F^{(0)}$  is in very good agreement with the exact simulation for small values of  $T$  (Appendix E discusses the choice of the lowest period). The existence of almost strong edge modes in this setting, corresponds to the generalization of the results of Kemp et al<sup>7</sup> to a quantum quench, for which the system thermalizes on short, system-size independent time-scales, while the zero mode persists over a much larger time-scale.

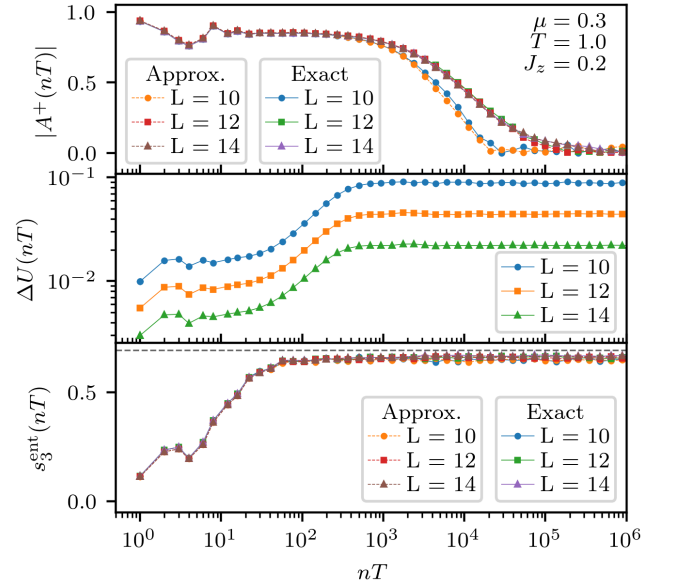


FIG. 11. Dynamics of almost strong zero mode. Top row:  $A^+(nT)$  for the exact  $U$  and for the approximate  $U_{\text{approx}}$  given by the leading order Magnus expansion. Middle row:  $\Delta U(nT)$  as a function of the entanglement cut as a function of stroboscopic time. Bottom row: Time evolution of the entanglement entropy density for a quench from a Néel state. The entanglement cut is placed after the third site from the left end of the chain. The onset of the decay for the almost strong zero modes is not tied to the short time features in  $\Delta U$  or  $s_3^{\text{ent}}$ . Lowering  $J_z$  to 0.1 (not shown) pushes the onset of the decay out to  $10^5$  periods while the steady states of the middle and bottom panels saturate before  $10^3$  and  $10^2$  respectively.

In the low frequency regime we can analyze the vicinity of the exactly solvable limit  $J_z = 0$ ,  $T\mu/3 = \pi/2$  which supports a strong  $\pi$ -mode. The Floquet Hamiltonian at this point is  $TH_F^{(1)} = \frac{TJ_x}{3} H_{xx} + \frac{\pi}{2} \mathcal{D}$ , and  $\sigma_1^x$  is an exact strong  $\pi$ -mode operator. Setting  $J_z T/3 = \delta_{zz} \sim 0.082$ ,  $T\mu/3 = \pi/2 + \delta_z \sim \pi/2 - 0.015$ , and  $J_x T/3 = \pi/4 + 0.1/3 = \theta_x$ , we note that we cannot

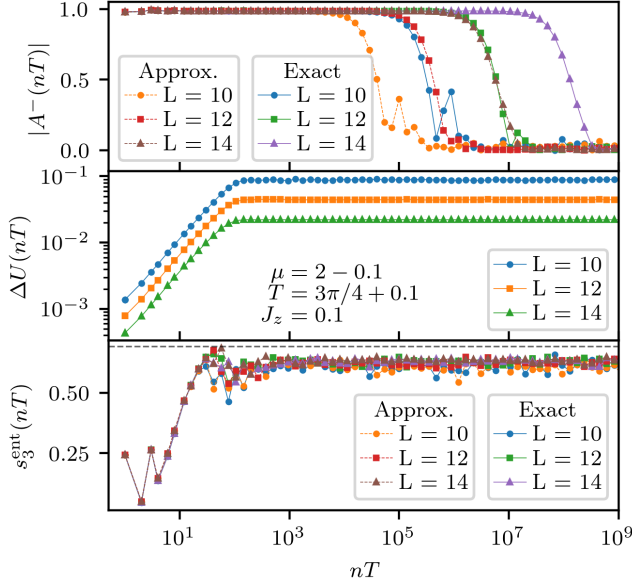


FIG. 12. Top panel: Overlap  $A^-(nT)$  showing an almost strong  $\pi$  mode for both the exact time evolution and the approximate  $H_F$ , the latter given by a BCH expansion about the point  $T\mu/3 = \pi/2 + \delta_z, TJ_x/3 = \pi/4 + \delta_T, TJ_z/3 = \delta_{zz}$ . Here,  $\delta_T = 0.1/3$ ,  $\delta_z \sim -0.015$ ,  $\delta_{zz} \sim 0.082$ . Middle panel:  $\Delta U(nT)$  as a function of stroboscopic time. Bottom panel: Time evolution of the entanglement entropy density with the entanglement cut placed after the third site from the left end of the chain. The initial state is a Néel state. While the expression for  $H_F$  fails to capture the long time dynamics accurately, it nevertheless manages to capture the exponential in system size dependence of the lifetime of the almost strong mode. We stress that the agreement of the exact  $L = 12$  and approximate  $L = 14$  results in the top panel is purely coincidental.

perform a high-frequency expansion as  $TJ_x$  is not small. Nevertheless,  $H_F$  to first order in  $\delta_{zz}, \delta_z$  but to arbitrary orders in  $TJ_x$  may be derived from an infinite resummation of the Baker-Campbell-Hausdorff formula to obtain a non-local perturbed Ising model (see Appendix D),

$$\begin{aligned}
 TH_F^{(1)} \sim & \frac{TJ_x}{3} H_{xx} + \frac{\pi}{2} \mathcal{D} + \delta_{zz} [a_1 (h_{zyx} + h_{xyz}) \\
 & + a_2 h_{zz}^E + a_3 h_{zz}^B + a_4 h_{xyyx}] + \delta_z [b_1 h_z^E + b_2 h_z^B \\
 & + b_3 h_{xx} + b_4 (h_{xy} + h_{yx})].
 \end{aligned} \quad (10)$$

Here we have defined  $h_{\alpha_1 \dots \alpha_k} = \sum_j \sigma_j^{\alpha_1} \dots \sigma_{j+k-1}^{\alpha_k} \equiv h_{\alpha_1 \dots \alpha_k}^E + h_{\alpha_1 \dots \alpha_k}^B$ , where  $h^E$  denotes the contribution involving the spins  $\sigma_{1,L}^{\alpha}$  and  $h^B$  the bulk part. As expected, these additional terms still commute with  $\mathcal{D}$ . Fig. 12 shows that the dynamics of  $A^-(nT)$  generated by this Hamiltonian qualitatively agrees with the exact time evolution despite  $\Delta U$  growing large at shorter times. Taking into account higher order corrections in  $\delta_{zz}, \delta_z$ <sup>46</sup> is expected to improve this agreement as long as we are close enough to the exactly solvable point  $\delta_{zz}, \delta_z \ll 1$ .

## V. CONCLUSIONS

We have established the existence of long-lived edge modes in periodically driven disorder-free systems with interacting Floquet Hamiltonians. The lifetimes of these edge modes are much longer than the time scales over which the system heats to infinite temperature. This complements known results for edge modes in periodically driven disordered and prethermal systems. The existence of these modes imply robust edge states that survive heating, and open up the possibility of using these states in quantum information and computing.

Our work raises a number of questions. Most importantly one should understand what determines the lifetimes of the almost strong zero and  $\pi$  modes. This is currently under investigation. Another question is to what extent our findings can be understood in terms of Ref. 44 where the authors give precise statements on the lifetime of prethermal physics for driven systems at high frequencies. In this paper, we avoided this regime due to the limits in system sizes accessible to us. To investigate this one should understand in what parameter regime expansions of the Floquet Hamiltonian around solvable limits are asymptotic to sufficiently high orders. It also would be interesting to explore eigenspectrum phases with (almost) strong edge modes in spin-1 chains and higher dimensional equilibrium as well as periodically driven systems. Other questions are whether the strong edge modes in all free Floquet SPTs<sup>19,31–33,47–50</sup> are equally robust to adding interactions. It is also interesting to explore the connection between almost strong mode operators in interacting Floquet Hamiltonians and edge modes of interacting topological phases<sup>51,52</sup>.

**Acknowledgements:** We are grateful to Paul Fendley, Robert Konik, Sid Parameswaran and Sthitadhi Roy for very helpful discussions. This work was supported by the US Department of Energy, Office of Science, Basic Energy Sciences, under Award No. de-sc0010821 (D.J.Y. and A.M.), and by the EPSRC under Grant No. EP/N01930X (F.H.L.E.). A.M. and F.H.L.E. also thank KITP for hospitality, which is supported by the National Science Foundation under Grant No. NSF PHY-1748958.

### Appendix A: Explicit construction of the strong $0, \pi$ mode operators for the binary drive

Our starting point is the time evolution of Majorana operators under the two unitaries of our binary drive. Defining

$$\begin{aligned}
 U_1(T) &= e^{-i\mu H_z \frac{T}{2}}, \\
 U_2(T) &= e^{-iJ_x H_{xx} \frac{T}{2}},
 \end{aligned} \quad (A1)$$

we have

$$U_1^\dagger(T) a_{2j} U_1(T) = \cos(T\mu) a_{2j} + \sin(T\mu) a_{2j-1}, \quad (A2)$$

$$U_1^\dagger(T) a_{2j-1} U_1(T) = \cos(T\mu) a_{2j-1} - \sin(T\mu) a_{2j}, \quad (A3)$$



$$U_2^\dagger(T) a_{2j} U_2(T) = \begin{cases} a_{2j} & j = L \\ \cos(TJ_x) a_{2j} - \sin(TJ_x) a_{2j+1} & j < L. \end{cases}, \quad (\text{A4})$$

$$U_2^\dagger(T) a_{2j-1} U_2(T) = \begin{cases} a_{2j-1} & j = 1 \\ \cos(TJ_x) a_{2j-1} + \sin(TJ_x) a_{2j-2} & j > 1. \end{cases} \quad (\text{A5})$$

Denoting the time evolved Majorana operators by  $a_j(nT) = U^\dagger(nT) a_j U(nT)$ , we can cast the evolution equations in the form

$$\begin{pmatrix} \vec{a}_{\text{odd}}((n+1)T) \\ \vec{a}_{\text{even}}((n+1)T) \end{pmatrix} \equiv M \begin{pmatrix} \vec{a}_{\text{odd}}(nT) \\ \vec{a}_{\text{even}}(nT) \end{pmatrix}, \quad (\text{A6})$$

where  $\vec{a}_{\text{odd}}(nT) = (a_1(nT), a_3(nT), \dots, a_{2L-1}(nT))$ ,  $\vec{a}_{\text{even}}(nT) = (a_2(nT), a_4(nT), \dots, a_{2L}(nT))$  and

$$M = \left( \begin{array}{cc|cc} a' & & c' & \\ b & a & -d & c \\ & \ddots & \ddots & \\ -c & d & a & b \\ & \ddots & \ddots & \\ & & -c' & a' \end{array} \right), \quad (\text{A7})$$

and

$$\begin{aligned} a &= \cos(T\mu) \cos(TJ_x), \quad b = \sin(T\mu) \sin(TJ_x), \\ c &= -\sin(T\mu) \cos(TJ_x), \quad d = -\cos(T\mu) \sin(TJ_x), \\ a' &= \cos(T\mu), \quad c' = -\sin(T\mu). \end{aligned} \quad (\text{A8})$$

We now use that the spin operators at the left edge of the chain have a simple expression in terms of the Majorana fermions, i.e.  $\sigma_1^x(0) = a_1(0)$ . This suggests the following Ansatz for the zero and  $\pi$  mode operators

$$\Psi_\sigma = \sum_{j=1}^L \psi_j^{(\sigma)} a_{2j-1} + \phi_j^{(\sigma)} a_{2j}, \quad (\text{A9})$$

where  $\phi_j^{(\sigma)}$  and  $\psi_j^{(\sigma)}$  are respectively the amplitudes of the expansion for the even and odd Majorana sublattices. The requirement that

$$U^\dagger(T) \Psi_\sigma U(T) = \cos(\sigma) \Psi_\sigma, \quad (\text{A10})$$

translates into an eigenvalue equation for  $M^T$

$$M^T \begin{pmatrix} \vec{\psi} \\ \vec{\phi} \end{pmatrix} = \cos(\sigma) \begin{pmatrix} \vec{\psi} \\ \vec{\phi} \end{pmatrix}. \quad (\text{A11})$$

As  $M^T$  is an orthogonal matrix we can equivalently consider the eigenvalue equation for  $M$ , which we do in the following. Denoting the  $L \times L$  blocks of  $M$  by

$$M = \begin{pmatrix} M_1 & M_2 \\ -\mathbb{F} M_2 \mathbb{F} & \mathbb{F} M_1 \mathbb{F} \end{pmatrix}, \quad \mathbb{F} = \begin{pmatrix} & 1 \\ & 1 \\ \ddots & \end{pmatrix}, \quad (\text{A12})$$

we can block-diagonalize  $M$  by

$$\tilde{M} = \mathcal{U} M \mathcal{U}^\dagger, \quad \mathcal{U} = \frac{1}{\sqrt{2}} \begin{pmatrix} \mathbb{I} & i\mathbb{F} \\ \mathbb{I} & -i\mathbb{F} \end{pmatrix}. \quad (\text{A13})$$

This gives

$$\tilde{M} = \begin{pmatrix} \tilde{M}_1 & \\ & \tilde{M}_2 \end{pmatrix} = \begin{pmatrix} M_1 - iM_2 \mathbb{F} & \\ & M_1 + iM_2 \mathbb{F} \end{pmatrix}. \quad (\text{A14})$$

Finally we may diagonalize  $\tilde{M}_i = V_i \Lambda_i V_i^\dagger$ , where  $\Lambda_i$  is the diagonal matrix of eigenvalues and the columns of  $V_i$  host the eigenvectors. Putting everything together we can express  $M$  in the form

$$\begin{aligned} M &= \frac{1}{\sqrt{2}} \begin{pmatrix} V_1 & V_2 \\ -i\mathbb{F} V_1 & i\mathbb{F} V_2 \end{pmatrix} \begin{pmatrix} \Lambda_1 & \\ & \Lambda_2 \end{pmatrix} \frac{1}{\sqrt{2}} \begin{pmatrix} V_1^\dagger & iV_1^\dagger \mathbb{F} \\ V_2^\dagger & -iV_2^\dagger \mathbb{F} \end{pmatrix} \\ &\equiv W \Lambda W^\dagger. \end{aligned} \quad (\text{A15})$$

Since  $\tilde{M}_1^* = \tilde{M}_2$  and  $M$  is orthogonal, for each eigenvector  $|\lambda\rangle$  of  $\tilde{M}_1$ , there is an eigenvector  $|\lambda^*\rangle$  of  $\tilde{M}_2$ . For this reason, it suffices to focus on  $\tilde{M}_1$ . In the limit of large system size the eigenvalue equation for  $\tilde{M}_1$  turns into a matrix recurrence relation of the form ( $1 \leq j < L/2$ )

$$\begin{pmatrix} b & id \\ -ic & a - \lambda \end{pmatrix} \begin{pmatrix} \psi_j \\ \phi_{L+1-j} \end{pmatrix} + \begin{pmatrix} a - \lambda & -ic \\ id & b \end{pmatrix} \begin{pmatrix} \psi_{j+1} \\ \phi_{L-j} \end{pmatrix} = 0, \quad (\text{A16})$$

while for  $j = 1$  we have

$$\begin{pmatrix} a' - \lambda & -ic' \\ 0 & 0 \end{pmatrix} \begin{pmatrix} \psi_1 \\ \phi_L \end{pmatrix} = 0. \quad (\text{A17})$$

Assuming that  $T\mu \neq \mathbb{Z}\pi$ ,  $TJ_x \neq \mathbb{Z}\pi$  we can rewrite this in the form

$$\begin{pmatrix} \psi_{j+1} \\ \phi_{L-j} \end{pmatrix} = C \begin{pmatrix} \psi_j \\ \phi_{L+1-j} \end{pmatrix}, \quad j \geq 1, \quad (\text{A18})$$

where the matrix  $C$  is

$$C = \frac{1}{\lambda \sin(T\mu) \sin(TJ_x)} \begin{pmatrix} \sin^2(T\mu) & -i[-\lambda \cos(J_x T) + \cos(T\mu)] \sin(T\mu) \\ i[-\lambda \cos(J_x T) + \cos(T\mu)] \sin(T\mu) & 1 - 2\lambda \cos(J_x T) \cos(T\mu) + \cos^2(T\mu) \end{pmatrix} \quad (\text{A19})$$

The eigenvalues of  $C$ , for a given  $\lambda$  are

$$\tilde{\epsilon}_{\pm} = \delta_{\lambda, \pm 1} [\cot(T\mu/2) \tan(TJ_x/2)]^{\pm 1} - \delta_{\lambda, -1} [\cot(T\mu/2) \cot(TJ_x/2)]^{\pm 1}. \quad (\text{A20})$$

The eigenvectors of  $C$  are,

$$|\tilde{\epsilon}_+\rangle = \begin{pmatrix} -i \sin(T\mu/2) \\ \cos(T\mu/2) \end{pmatrix}, \quad |\tilde{\epsilon}_-\rangle = \begin{pmatrix} \cos(T\mu/2) \\ -i \sin(T\mu/2) \end{pmatrix}, \quad (\text{A21})$$

and are independent of  $\lambda$ . The solutions to (A17) for the relevant eigenvalues  $\lambda = \pm 1$  are

$$\begin{pmatrix} \psi_1 \\ \phi_L \end{pmatrix} = \begin{cases} |\tilde{\epsilon}_-\rangle & \text{if } \lambda = 1 \\ |\tilde{\epsilon}_+\rangle & \text{if } \lambda = -1 \end{cases}. \quad (\text{A22})$$

It is convenient to define,

$$\epsilon_{\pm} = \mp \frac{[\cot(T\mu/2)]^{\pm 1}}{\tan(TJ_x/2)}. \quad (\text{A23})$$

Using the eigen-decomposition of  $C$  in (A18), we conclude that

$$\begin{pmatrix} \psi_{n+1} \\ \phi_{L-n} \end{pmatrix} = \delta_{\lambda, 1} \begin{pmatrix} \cos(T\mu/2) \\ -i \sin(T\mu/2) \end{pmatrix} \epsilon_-^n + \delta_{\lambda, -1} \begin{pmatrix} -i \sin(T\mu/2) \\ \cos(T\mu/2) \end{pmatrix} \epsilon_+^n. \quad (\text{A24a})$$

So far we have neglected the fact that for  $j = L/2$  the set of recurrence relations is different. This is justified as long as  $|\epsilon_{\pm}| < 1$  and  $L \gg 1$ . In this regime we can decompose the zero and  $\pi$  modes into their respective contributions centered on the left and right edges respectively  $\Psi_{0,\pi} \approx \Psi_{0,\pi}^L + \Psi_{0,\pi}^R$ . Focusing only on the left edge we have

$$\begin{aligned} \Psi_0^L &\approx \sum_{j \geq 1} \epsilon_-^{j-1} \left[ \cos\left(\frac{T\mu}{2}\right) a_{2j-1} - \sin\left(\frac{T\mu}{2}\right) a_{2j} \right], \\ \Psi_{\pi}^L &\approx \sum_{j \geq 1} \epsilon_+^{j-1} \left[ \sin\left(\frac{T\mu}{2}\right) a_{2j-1} + \cos\left(\frac{T\mu}{2}\right) a_{2j} \right]. \end{aligned} \quad (\text{A25})$$

These are the expressions given in the main text.

## Appendix B: Edge mode diagnostic $A(nT)$

In this subsection we discuss the two measures  $A(nT), A_{\psi}(nT)$  used to identify almost strong edge

modes. The time evolution operators commutes with rotations around the  $z$ -axis by 180 degrees, and we therefore can choose the eigenstates of  $U(T)$  to have definite parity under these  $\mathbb{Z}_2$  transformations

$$\begin{aligned} U(T)|m\rangle &= e^{-iT\epsilon_m}|m\rangle, \\ \mathcal{D}|m\rangle &= s_m|m\rangle, \quad s_m = \pm 1. \end{aligned} \quad (\text{B1})$$

Up to finite-size corrections exponentially small in system size a strong zero mode  $\Psi_0$  sends eigenstates to eigenstates with degenerate eigenvalues but with the opposite eigenvalue for  $\mathcal{D}$

$$\Psi_0|m\rangle \approx |\bar{m}\rangle, \quad \epsilon_{\bar{m}} \approx \epsilon_m, \quad (\text{B2})$$

A strong  $\pi$  mode behaves similarly except that the quasi-energies are shifted by  $\pi/T$ . The spectral representation of  $A(nT)$  reads

$$A(nT) = \frac{1}{2^L} \sum_{m_1, m_2} |\langle m_1 | \sigma_1^x | m_2 \rangle|^2 e^{-i(\epsilon_{m_2} - \epsilon_{m_1})nT}. \quad (\text{B3})$$

As  $\sigma_1^x$  is odd under the  $\mathbb{Z}_2$  we have

$$\sigma_1^x = c_0 \Psi_0 + c_{\pi} \Psi_{\pi} + \dots \quad (\text{B4})$$

The coefficients  $c_0$  and  $c_{\pi}$  are different from zero only if strong zero/ $\pi$  modes exist. Substituting this into the spectral representation we have

$$\begin{aligned} A(nT) &= \frac{|c_0|^2}{2^L} \sum_{m_1, m_2} |\langle m_1 | \Psi_0 | m_2 \rangle|^2 e^{-i(\epsilon_{m_2} - \epsilon_{m_1})nT} \\ &+ \frac{|c_{\pi}|^2}{2^L} \sum_{m_1, m_2} |\langle m_1 | \Psi_{\pi} | m_2 \rangle|^2 e^{-i(\epsilon_{m_2} - \epsilon_{m_1})nT} \\ &+ \frac{1}{2^L} \sum_{m_1, m_2} \left[ c_0^* c_{\pi} \langle m_1 | \Psi_0 | m_2 \rangle \right. \\ &\quad \left. \times \langle m_2 | \Psi_{\pi} | m_1 \rangle + \text{h.c.} \right] e^{-i(\epsilon_{m_2} - \epsilon_{m_1})nT} + \dots \end{aligned} \quad (\text{B5a})$$

The exponential factors in (B5a) will be strongly oscillating for large  $nT$  except for the  $2^L$  terms in the double sums that correspond to “paired” states (B2) and their  $\pi$ -mode analogues. By the same arguments used in the thermalization context, the time average of the sum over oscillating terms becomes negligible at late times. Assuming that  $A(nT)$  relaxes, the oscillatory terms will therefore not contribute to the late-time behavior and

$$A(nT) \approx |c_0|^2 + |c_{\pi}|^2 e^{-i\pi n}. \quad (\text{B6})$$

The second measure we use is defined with respect to an initial state  $|\psi\rangle$

$$A_\psi(nT) = \langle \psi | U(nT)^\dagger \sigma_1^x U(nT) \sigma_1^x | \psi \rangle. \quad (\text{B7})$$

The physical meaning of this quantity is that we start from an initial state  $|\psi\rangle$ , flip a spin at site 1, then time-evolve until time  $nT$ , and flip the spin back again obtaining a state  $\sigma_1^x U(nT) \sigma_1^x | \psi \rangle$ .  $A_\psi(nT)$  then measures the overlap of this state with one where the initial state was evolved up to time  $nT$  without the initial spin-flip  $U(nT)|\psi\rangle$ . Employing a spectral representation we have

$$A_\psi(nT) = \sum_{m_1, m_2} \langle m_1 | \sigma_1^x | m_2 \rangle e^{-i(\epsilon_{m_2} - \epsilon_{m_1})nT} \times \langle \psi | m_1 \rangle \langle m_2 | \sigma_1^x | \psi \rangle. \quad (\text{B8})$$

Focussing on the non-oscillatory terms in this double sum (modulo  $(-1)^n$  in case of the  $\pi$ -mode) gives a late time contribution that is the same as (B6)

$$A_\psi(nT) \approx |c_0|^2 + |c_\pi|^2 (-1)^n. \quad (\text{B9})$$

In Fig. 13 we show the time-evolution of the symmetrized autocorrelation functions  $A^+(nT), A_\psi^+(nT)$ , and where  $|\psi\rangle$  is chosen to be the Néel state. The figure shows that an almost strong zero mode exists, and that the agreement between the two measures is good.

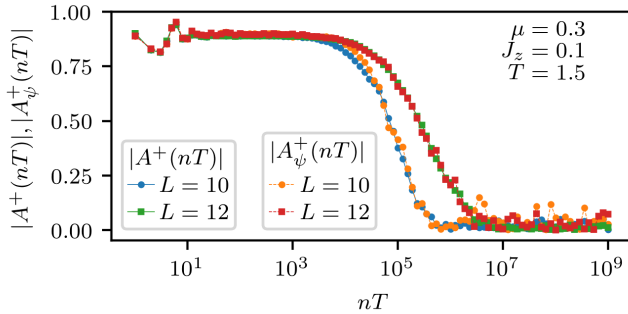


FIG. 13. Symmetrized overlaps  $A^+(nT), A_\psi^+(nT)$ , where  $|\psi\rangle$  is the Néel state. The time-evolution of the two quantities are almost identical, with both showing a lifetime that grows with system size  $L$ , indicating an almost strong zero mode.

### Appendix C: System size dependence of the phase diagram

Fig. 14 plots two metrics for the almost strong modes  $\Gamma, \chi$ , each formally defined in the caption.  $\Gamma$  measures the extent to which the operator  $\sigma_1^x$  connects different quasi-energy states, and does not differentiate between whether these states have degenerate quasi-energies or not.

$\chi$  measures the level of degeneracy for almost strong modes and/or the level to which energies are separated

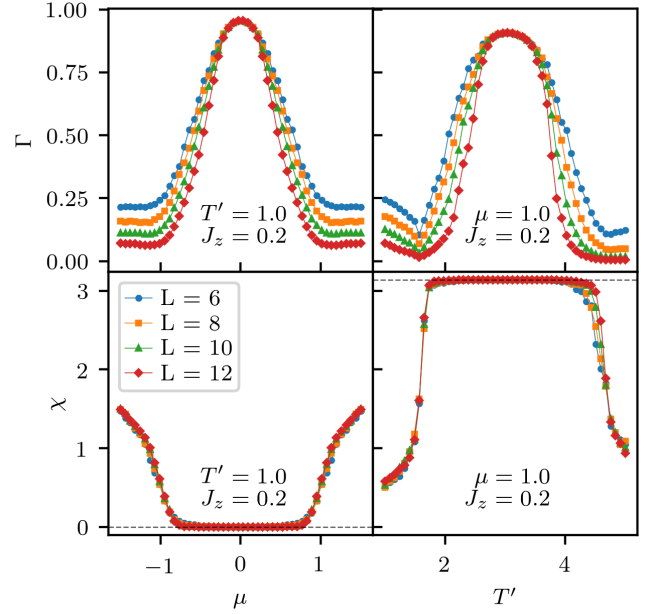


FIG. 14. Top panels: Plots of  $\Gamma = \text{mean}_s \max_{s'} |\langle s | \sigma_1^x | s' \rangle|^2$  where values of  $O(1)$  indicate an almost strong zero mode (left panel) or almost strong  $\pi$  mode (right panel). The nontrivial edge phases are robust to system size. Lower panels show another metric from directly measuring the pairing structure of the quasi-energy spectrum of the Floquet unitary. Lower left panel: Denoting  $|s'\rangle$  as the state that maximizes  $|\langle s | \sigma_1^x | s' \rangle|^2$  for a given state  $|s\rangle$ ,  $\chi = \text{mean}_s |\text{angle}(T\epsilon_s, T\epsilon_{s'})|$  for both almost strong 0 mode (left panel) and almost strong  $\pi$  mode (right panel).  $\text{angle}(x, y)$  finds the (smaller) angle between the two points on the unit circle. Note that while  $\Gamma$  cannot distinguish between 0,  $\pi$  modes,  $\chi$  can.

by  $\pi/T$ . The plots show that deep within the phases, there is negligible system size dependence.

We have taken care to pick phases where only almost strong 0 or almost strong  $\pi$  mode exists, but  $\chi$  can also identify phases when both are present simultaneously. A flat plateau in  $\chi$  away from 0,  $\pi$  would indicate the presence of coexisting 0 -  $\pi$  modes.

### Appendix D: Derivation of Floquet Hamiltonian with almost strong $\pi$ mode

We outline the derivation of  $H_F$ , for the ternary drive, around the exactly solvable limit  $J_z = 0, T\mu/3 = \pi/2$ . Setting,  $J_z T/3 = \delta_{zz}$ ,  $T\mu/3 = \pi/2 + \delta_z$ , and  $J_x T/3 = \pi/4 + 0.1/3 = \theta_x$ , the Floquet unitary may be written as,

$$U(T) = e^{-iH_F T} = e^{-i\frac{TJ_z}{3}H_{zz}} e^{-i\frac{TJ_x}{3}H_{xx}} e^{-i\frac{T\mu}{3}H_z}, \quad (\text{D1a})$$

$$\equiv (-i)^{L-1} e^{-i\delta_{zz}H_{zz}} e^{-i\theta_x H_{xx}} e^{-i\delta_z H_z} e^{-i\frac{\pi}{2}\mathcal{D}}, \quad (\text{D1b})$$

where in the last line we have used that  $e^{-i\pi H_z/2} = (-i)^L \mathcal{D} = (-i)^{L-1} e^{-i\frac{\pi}{2}\mathcal{D}}$ . These steps are carried out

to explicitly show that we have a Floquet Hamiltonian that is non-local, and that it is in fact the presence or absence of non-local term  $\mathcal{D}$  in the Floquet Hamiltonian that determines whether  $\sigma_1^x$  is respectively a strong  $\pi$  mode or a strong 0 mode.

In what follows we will consider the limit of  $\delta_{zz}, \delta_z \ll 1$ . We use the following formula from Baker-Campbell-

Hausdorff (BCH),

$$\log(\exp(X)\exp(Y)) = X + \frac{\text{ad}_X \text{ad}_Y}{e^{\text{ad}_X} - 1} Y + \mathcal{O}(Y^2). \quad (\text{D2})$$

Furthermore, we use the following identity,

$$\frac{t}{1 - e^{-t}} = \sum_{m=0}^{\infty} \frac{B_m^+ t^m}{m!}, \quad (\text{D3})$$

where  $B_m^+$  are the Bernoulli numbers with  $B_1 = +\frac{1}{2}$ . We first note that  $\mathcal{D}$  commutes with everything, so it can be appended at the end of the calculation. We first combine the exponentials containing  $\theta_x H_{xx}$  and  $\delta_z H_z$ , and define the resulting operator as  $Z_1$ ,

$$-iZ_1 \sim -i\theta_x H_{xx} - i\delta_z \left( \sum_{n=0}^{\infty} \frac{B_n^+ (-i\theta_x \text{ad}_{H_{xx}})^n}{n!} \right) H_z + \mathcal{O}(\delta_z^2), \quad (\text{D4a})$$

$$\begin{aligned} &\sim -i\theta_x H_{xx} - i\delta_z \left\{ (\sigma_1^z + \sigma_L^z) \theta_x \cot(\theta_x) + \left( \frac{1 + 2\theta_x \cot(2\theta_x)}{2} \right) \sum_{i=2}^{L-1} \sigma_i^z \right. \\ &\quad \left. + \left( \frac{-1 + 2\theta_x \cot(2\theta_x)}{2} \right) \sum_{i=2}^{L-2} \sigma_{i-1}^x \sigma_i^z \sigma_{i+1}^x - \theta_x \sum_{i=1}^{L-1} (\sigma_i^x \sigma_{i+1}^y + \sigma_i^y \sigma_{i+1}^x) \right\}, \end{aligned} \quad (\text{D4b})$$

$$\equiv -i\theta_x H_{xx} - i\delta_z \left\{ h_z^E \theta_x \cot(\theta_x) + h_z^B \left( \frac{1 + 2\theta_x \cot(2\theta_x)}{2} \right) + h_{xxz} \left( \frac{-1 + 2\theta_x \cot(2\theta_x)}{2} \right) - \theta_x (h_{xy} + h_{yx}) \right\}. \quad (\text{D4c})$$

Above we have used the notation  $h_{\alpha_1 \dots \alpha_k} = \sum_j \sigma_j^{\alpha_1} \dots \sigma_{j+k-1}^{\alpha_k} \equiv h_{\alpha_1 \dots \alpha_k}^E + h_{\alpha_1 \dots \alpha_k}^B$ , where  $h^E$  denotes the contribution involving the spins  $\sigma_{1,L}^\alpha$  and  $h^B$  the bulk

part.

Next we combine the  $H_{zz}$  and  $Z_1$  exponentials using the same steps as above, and only working to first order in  $\delta_z, \delta_{zz}$ , obtain the resulting operator  $Z_2$

$$\begin{aligned} -iZ_2 &\sim -iZ_1 - i\delta_{zz} \left\{ (\sigma_1^z \sigma_2^z + \sigma_{L-1}^z \sigma_L^z) \theta_x \cot(\theta_x) + \left( \frac{1 + 2\theta_x \cot(2\theta_x)}{2} \right) \sum_{i=2}^{L-2} \sigma_i^z \sigma_{i+1}^z \right. \\ &\quad \left. - \left( \frac{-1 + 2\theta_x \cot(2\theta_x)}{2} \right) \sum_{i=2}^{L-2} (\sigma_{i-1}^x \sigma_i^y \sigma_{i+1}^y \sigma_{i+2}^x) + \theta_x \sum_{i=2}^{L-1} (\sigma_{i-1}^z \sigma_i^y \sigma_{i+1}^x + \sigma_{i-1}^x \sigma_i^y \sigma_{i+1}^z) \right\}, \end{aligned} \quad (\text{D5a})$$

$$\equiv -iZ_1 - i\delta_{zz} \left\{ h_{zz}^E \theta_x \cot(\theta_x) + h_{zz}^B \left( \frac{1 + 2\theta_x \cot(2\theta_x)}{2} \right) - h_{xyyz} \left( \frac{-1 + 2\theta_x \cot(2\theta_x)}{2} \right) + \theta_x (h_{zyx} + h_{xyz}) \right\}. \quad (\text{D5b})$$

Now including the  $\pi\mathcal{D}/2$  term, we have our approximate

$H_F$ ,

$$\begin{aligned}
TH_F \sim & \theta_x H_{xx} + \frac{\pi}{2} \mathcal{D} + \delta_z \left\{ h_z^E \theta_x \cot(\theta_x) + h_z^B \left( \frac{1 + 2\theta_x \cot(2\theta_x)}{2} \right) + h_{xzx} \left( \frac{-1 + 2\theta_x \cot(2\theta_x)}{2} \right) - \theta_x (h_{xy} + h_{yx}) \right\} \\
& + \delta_{zz} \left\{ h_{zz}^E \theta_x \cot(\theta_x) + h_{zz}^B \left( \frac{1 + 2\theta_x \cot(2\theta_x)}{2} \right) - h_{xyyx} \left( \frac{-1 + 2\theta_x \cot(2\theta_x)}{2} \right) + \theta_x (h_{zyx} + h_{xyz}) \right\}. \quad (\text{D6})
\end{aligned}$$

As we are working only to first order in  $\delta_z, \delta_{zz}$  we expect this  $H_F$  to only be valid for short times.

While we have used the BCH formula above, a more systematic approach following the methods in Ref. 46 could prove useful for higher orders. In fact we have checked that using the alternative approach of 46, and working to first order gives the same form of  $H_F$ .

### Appendix E: Discussion of parameters used

Fig. 15 shows how the many-particle quasi-energy spectrum evolves with system size  $L$ . For any  $T$ , too small a system will not capture any true Floquet dynamics as the spectrum will not reach the Floquet zone boundaries, and the system will always appear highly off-resonant. For the parameters of our paper,  $T = 1$  is a reasonable lower limit for the period. As a general rule, for a given  $T$ , increasing  $J_z$  or  $L$  or both, increases the number of many-body resonances.

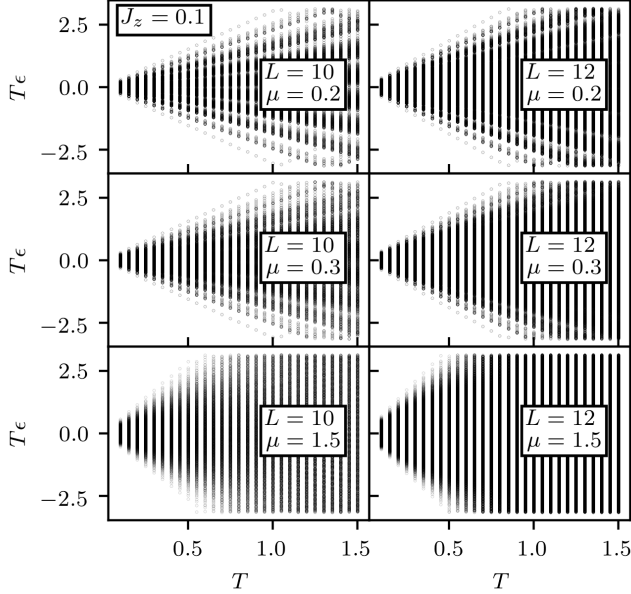


FIG. 15. Quasi-energy spectrum plotted against  $T$  for select  $\mu$  values. For small system sizes, setting  $T$  too small can lead to the drive being off-resonant with the extensive many-body spectrum. We see that for  $L = 12$ ,  $T = 1$  is a reasonable lower limit for our calculations.



- <sup>1</sup> A. Kitaev, *Annals of Physics* **321**, 2 (2006), january Special Issue.
- <sup>2</sup> C. Nayak, S. H. Simon, A. Stern, M. Freedman, and S. Das Sarma, *Rev. Mod. Phys.* **80**, 1083 (2008).
- <sup>3</sup> P. Fendley, M. P. Fisher, and C. Nayak, *Annals of Physics* **324**, 1547 (2009), july 2009 Special Issue.
- <sup>4</sup> J. Alicea, *Reports on Progress in Physics* **75**, 076501 (2012).
- <sup>5</sup> C. Beenakker, *Annual Review of Condensed Matter Physics* **4**, 113 (2013).
- <sup>6</sup> P. Fendley, *Journal of Physics A: Mathematical and Theoretical* **49**, 30LT01 (2016).
- <sup>7</sup> J. Kemp, N. Y. Yao, C. R. Laumann, and P. Fendley, *Journal of Statistical Mechanics: Theory and Experiment* **2017**, 063105 (2017).
- <sup>8</sup> D. V. Else, P. Fendley, J. Kemp, and C. Nayak, *Phys. Rev. X* **7**, 041062 (2017).
- <sup>9</sup> L. M. Vasiloiu, F. Carollo, and J. P. Garrahan, *Phys. Rev. B* **98**, 094308 (2018).
- <sup>10</sup> L. M. Vasiloiu, F. Carollo, M. Marcuzzi, and J. P. Garrahan, arXiv:1901.10211 (unpublished).
- <sup>11</sup> M. Thakurathi, A. A. Patel, D. Sen, and A. Dutta, *Phys. Rev. B* **88**, 155133 (2013).
- <sup>12</sup> Y. Bahri, R. Ronen, E. Altman, and A. Vishwanath, *Nature Communications* **6**, 7341 (2015).
- <sup>13</sup> V. Khemani, A. Lazarides, R. Moessner, and S. L. Sondhi, *Phys. Rev. Lett.* **116**, 250401 (2016).
- <sup>14</sup> G. J. Sreejith, A. Lazarides, and R. Moessner, *Phys. Rev. B* **94**, 045127 (2016).
- <sup>15</sup> I.-D. Potirniche, A. C. Potter, M. Schleier-Smith, A. Vishwanath, and N. Y. Yao, *Phys. Rev. Lett.* **119**, 123601 (2017).
- <sup>16</sup> A. Kumar, P. T. Dumitrescu, and A. C. Potter, *Phys. Rev. B* **97**, 224302 (2018).
- <sup>17</sup> X.-G. Wen, *Rev. Mod. Phys.* **89**, 041004 (2017).
- <sup>18</sup> T. Iadecola, L. H. Santos, and C. Chamon, *Phys. Rev. B* **92**, 125107 (2015).
- <sup>19</sup> T. Kitagawa, E. Berg, M. Rudner, and E. Demler, *Phys. Rev. B* **82**, 235114 (2010).
- <sup>20</sup> A. C. Potter, T. Morimoto, and A. Vishwanath, *Phys. Rev. X* **6**, 041001 (2016).
- <sup>21</sup> D. V. Else and C. Nayak, *Phys. Rev. B* **93**, 201103(R) (2016).
- <sup>22</sup> R. Roy and F. Harper, *Phys. Rev. B* **94**, 125105 (2016).
- <sup>23</sup> C. W. von Keyserlingk and S. L. Sondhi, *Phys. Rev. B* **93**, 245145 (2016).
- <sup>24</sup> A. Chandran, V. Khemani, C. R. Laumann, and S. L. Sondhi, *Phys. Rev. B* **89**, 144201 (2014).
- <sup>25</sup> A. Lazarides, A. Das, and R. Moessner, *Phys. Rev. E* **90**, 012110 (2014).
- <sup>26</sup> H. Kim, T. N. Ikeda, and D. A. Huse, *Phys. Rev. E* **90**, 052105 (2014).
- <sup>27</sup> L. D'Alessio and M. Rigol, *Phys. Rev. X* **4**, 041048 (2014).
- <sup>28</sup> P. Ponte, A. Chandran, Z. Papi, and D. A. Abanin, *Annals of Physics* **353**, 196 (2015).
- <sup>29</sup> A. Haldar, R. Moessner, and A. Das, *Phys. Rev. B* **97**, 245122 (2018).
- <sup>30</sup> V. Gritsev and A. Polkovnikov, *SciPost Phys.* **2**, 021 (2017).
- <sup>31</sup> J. K. Asbóth, B. Tarasinski, and P. Delplace, *Phys. Rev. B* **90**, 125143 (2014).
- <sup>32</sup> D. J. Yates and A. Mitra, *Phys. Rev. B* **96**, 115108 (2017).
- <sup>33</sup> D. Yates, Y. Lemonik, and A. Mitra, *Phys. Rev. Lett.* **121**, 076802 (2018).
- <sup>34</sup> L. D'Alessio and A. Polkovnikov, *Annals of Physics* **333**, 19 (2013).
- <sup>35</sup> A. Eckardt and E. Anisimovas, *New Journal of Physics* **17**, 093039 (2015).
- <sup>36</sup> D. A. Abanin, W. De Roeck, and F. Huveneers, *Phys. Rev. Lett.* **115**, 256803 (2015).
- <sup>37</sup> B. Bertini, F. H. L. Essler, S. Groha, and N. J. Robinson, *Phys. Rev. Lett.* **115**, 180601 (2015).
- <sup>38</sup> A. Mitra, *Annual Review of Condensed Matter Physics* **9**, 245 (2018).
- <sup>39</sup> T. Kuwahara, T. Mori, and K. Saito, *Annals of Physics* **367**, 96 (2016).
- <sup>40</sup> M. Bukov, M. Heyl, D. A. Huse, and A. Polkovnikov, *Phys. Rev. B* **93**, 155132 (2016).
- <sup>41</sup> T. Mori, T. Kuwahara, and K. Saito, *Phys. Rev. Lett.* **116**, 120401 (2016).
- <sup>42</sup> D. V. Else, B. Bauer, and C. Nayak, *Phys. Rev. X* **7**, 011026 (2017).
- <sup>43</sup> D. A. Abanin, W. De Roeck, W. W. Ho, and F. Huveneers, *Phys. Rev. B* **95**, 014112 (2017).
- <sup>44</sup> D. Abanin, W. De Roeck, W. W. Ho, and F. Huveneers, *Communications in Mathematical Physics* **354**, 809 (2017).
- <sup>45</sup> F. H. L. Essler and M. Fagotti, *Journal of Statistical Mechanics: Theory and Experiment* **2016**, 064002 (2016).
- <sup>46</sup> S. Vajna, K. Klobas, T. Prosen, and A. Polkovnikov, *Phys. Rev. Lett.* **120**, 200607 (2018).
- <sup>47</sup> L. Jiang, T. Kitagawa, J. Alicea, A. R. Akhmerov, D. Pekker, G. Refael, J. I. Cirac, E. Demler, M. D. Lukin, and P. Zoller, *Phys. Rev. Lett.* **106**, 220402 (2011).
- <sup>48</sup> M. Benito, A. Gómez-León, V. M. Bastidas, T. Brandes, and G. Platero, *Phys. Rev. B* **90**, 205127 (2014).
- <sup>49</sup> W. Berdanier, M. Kolodrubetz, R. Vasseur, and J. E. Moore, *Phys. Rev. Lett.* **118**, 260602 (2017).
- <sup>50</sup> W. Berdanier, M. Kolodrubetz, S. A. Parameswaran, and R. Vasseur, *Proceedings of the National Academy of Sciences* **115**, 9491 (2018).
- <sup>51</sup> L. Fidkowski and A. Kitaev, *Phys. Rev. B* **83**, 075103 (2011).
- <sup>52</sup> R. Verresen, R. Moessner, and F. Pollmann, *Phys. Rev. B* **96**, 165124 (2017).